

Influence of pore roughness on high-frequency permeability

Andrea Cortis and David M. J. Smeulders

Delft University of Technology, P.O. Box 5028, 2600 GA Delft, The Netherlands

Jean Luc Guermond

Laboratoire d'Informatique pour la Mécanique et les Sciences de l'Ingénieur, UPR 3251 (CNRS), BP 133, 91403 Orsay, France

Denis Lafarge

Laboratoire d'Acoustique de l'Université du Maine, UMR 6613, Av. O. Messiaen, 72017 Le Mans, France

(Received 17 September 2002; accepted 24 February 2003; published 6 May 2003)

The high-frequency behavior of the fluid velocity patterns for smooth and corrugated pore channels is studied. The classical approach of Johnson *et al.* [J. Fluid Mech. **176**, 379 (1987)] for smooth geometries is obtained in different manners, thus clarifying differences with Sheng and Zhou [Phys. Rev. Lett. **61**, 1591 (1988)] and Avellaneda and Torquato [Phys. Fluids A **3**, 2529 (1991)]. For wedge-shaped pore geometries, the classical approach is modified by a nonanalytic extension proposed by Achdou and Avellaneda [Phys. Fluids A **4**, 2561 (1992)]. The dependency of the nonanalytic extension on the apex angle of the wedge was derived. Precise numerical computations for various apex angles in two-dimensional channels confirmed this theoretical dependency, which is somewhat different from the original Achdou and Avellaneda predictions. Moreover, it was found that the contribution of the singularities does not alter the parameters of the classical theory by Johnson *et al.* © 2003 American Institute of Physics. [DOI: 10.1063/1.1571545]

I. INTRODUCTION

The problem of fluid flow through porous media is of paramount importance in many technological areas. In air-filled sound absorbing media, a precise prediction of sound absorption versus frequency is needed.¹ In the oil industry, exploration wells are probed by acoustic tools and reservoir properties are delineated from the recorded wave trains.² The dynamic permeability $k(\omega)$, and the dynamic tortuosity $\alpha(\omega)$ are important properties to describe the macroscopic flow through porous media subjected to an oscillatory pressure gradient. Here, the term macroscopic refers to a length scale L that is much larger than any pore size a . Here L is defined as characteristic wavelength being the product of the fluid sound speed c , and an intrinsic viscous relaxation time a^2/ν , where ν is the kinematic viscosity of the pore fluid.^{1,3} Introducing an $\exp(i\omega t)$ dependence for the fluid pressure p and the macroscopic fluid velocity \mathbf{U} , $k(\omega)$ and $\alpha(\omega)$ are defined by

$$\frac{\eta\phi}{k(\omega)}\hat{\mathbf{U}} = -\nabla\hat{p}, \quad (1)$$

$$i\omega\rho_f\alpha(\omega)\hat{\mathbf{U}} = -\nabla\hat{p}. \quad (2)$$

In these two expressions, η is the fluid viscosity, ρ_f is the fluid density, and ϕ is the porosity. These relations take into account, in an averaged sense, the fluid motion that takes place in the pore structure, so that $k(\omega)$ and $\alpha(\omega)$ depend on the morphology of the pore space. Johnson *et al.*⁴ and later Sheng and Zhou⁵ and Zhou and Sheng,⁶ argued that the transition from low-frequency viscous behavior to high-frequency inertia behavior must be determined by the ratio

π_1 of the length scales $\sqrt{Fk_0}$ and δ . Here k_0 is the stationary Darcy permeability, and F is the formation factor, a nondimensional parameter that is related to the effective electrical conductivity of the porous medium saturated with a conductive fluid. The viscous skin depth $\delta = \sqrt{2\nu/\omega}$. It was consequently postulated that $k(\omega)$ satisfies a universally valid scaling function,

$$k(\omega) = k_0 f\left(\frac{Fk_0}{\delta^2}\right). \quad (3)$$

This also means that a characteristic frequency $\omega_c = \nu/Fk_0$ can be defined where the viscous forces and the inertia forces are of the same order of magnitude. Experimental work by Auriault *et al.*,⁷ Charlaix *et al.*,⁸ and Smeulders *et al.*³ show very good agreement of such theory on a wide variety of porous samples. A detailed theoretical analysis, however, showed that the structure function f of (3) must also depend on the ratio $\pi_2 = \delta/\Lambda$, where Λ is a pore volume-to-pore surface ratio weighted according to potential theory.⁴ Surprisingly, for a wide variety of morphologies, π_1 and π_2 were found not to be independent, i.e., their product was found to be $\sqrt{1/8}$, at least approximately. These morphologies had in common that they were smooth on the pore scale, i.e., the pore surface had bounded curvature. The possibility of departure from the structure function f for corrugated morphologies was investigated by several authors such as Kostek *et al.*,⁹ Smeulders *et al.*,¹⁰ Firdaouss *et al.*,¹¹ and Cortis and Smeulders.¹² It appeared that high values for $\pi_1 \times \pi_2$ could be reached for special cases, but these investigations still did not consider any comparison over the frequency domain. In other words, only the assumption that

$\pi_1 \times \pi_2 \approx \sqrt{1/8}$ was invalidated for some cases, but the structure function f could still be fully correct, if we rewrite it as a function of two parameters:^{3,4}

$$k(\omega) = k_0 f\left(\frac{Fk_0}{\delta^2}, \frac{Fk_0}{\Lambda^2}\right). \tag{4}$$

In a paper by Achdou and Avellaneda,¹³ however, departures from (4) were observed for microgeometries consisting of corrugated tubes. For high frequencies, they observed a slower convergence of $k(\omega)$ to its asymptotic limit than predicted from universality theory. A nonanalytic correction to the structure function (4) was proposed. Our aim in this paper is to study this nonanalytic correction factor. From microstructure, the dynamic permeability and tortuosity relations will be derived. Then, analyzing in detail the fluid velocity pattern in the bulk fluid and the boundary layer, the classical Johnson *et al.*⁴ high-frequency limit for smooth geometries will be obtained in different manners, making apparent the discrepancy with the Sheng and Zhou⁵ treatment, and clarifying the asymptotic boundary layer analysis proposed by Avellaneda and Torquato.¹⁴ For microgeometries consisting of corrugated tubes, this leads to a somewhat different high-frequency correction than proposed by Achdou and Avellaneda.¹³ Furthermore, the theoretical predictions will be numerically evaluated for two-dimensional channels that have wedge-shaped asperities.

II. OSCILLATING STOKES FLOW

Considering the unsteady Stokes equation for the fluid velocity field \mathbf{v} , we may write

$$i\omega\rho_f\hat{\mathbf{v}} = -\nabla\hat{p} + \eta\nabla^2\hat{\mathbf{v}} + \hat{\mathbf{g}}\mathbf{e}, \tag{5}$$

where \mathbf{e} is the unit vector (e_x, e_y, e_z), and $\hat{\mathbf{g}}$ is a spatially uniform oscillating source term, which is expressed in Nm^{-3} . In Achdou and Avellaneda,¹³ $\hat{\mathbf{g}}$ is an external oscillatory pressure gradient, which also appears quite naturally if the conventional technique of homogenization is used. Zhou and Sheng,⁶ Smeulders *et al.*,³ and Lafarge *et al.*¹ denote this externally applied pressure gradient $-\nabla_x p_0$. Indeed, the actual pressure p in the fluid can be viewed as the sum of its local mean value $p_0 = \langle p \rangle$ and its deviatoric part $\hat{p} = p - \langle p \rangle$, where $\langle \rangle$ denotes averaging over the pore fluid volume V_f . The local mean value p_0 varies at the macroscopic length scale L , thus its gradient may be considered a spatial constant in V_f . The deviatoric part \hat{p} varies at the pore scale a and is a compact field of zero mean value. This means that, on average, it does not increase or decrease in the direction of \mathbf{e} . It is fluctuating at the microscopic level because of the pore geometry, but it does not change from place to place when averages are considered. For periodic microstructures, the compact character of \hat{p} is expressed by periodic boundary conditions. Furthermore, it can be obtained from homogenization theory that, because of the scale separation $L \gg a$, the fluid is locally incompressible,

$$\nabla \cdot \hat{\mathbf{v}} = 0. \tag{6}$$

Introducing the scaled velocity $\tilde{\mathbf{v}} = \eta\hat{\mathbf{v}}/\hat{g}$ expressed in m^2 , and the scaled pressure $\tilde{p} = \hat{p}/\hat{g}$ expressed in m , the unsteady Stokes problem may be written as

$$i\omega\tilde{\mathbf{v}}/\nu = -\nabla\tilde{p} + \nabla^2\tilde{\mathbf{v}} + \mathbf{e}, \tag{7a}$$

$$\nabla \cdot \tilde{\mathbf{v}} = 0, \tag{7b}$$

$$\tilde{\mathbf{v}} = 0, \text{ on the pore walls,} \tag{7c}$$

$$\tilde{p}: \text{compact.} \tag{7d}$$

The solution to this problem can be expressed as a sum of normal modes:¹⁴

$$\tilde{\mathbf{v}}(\mathbf{r}, \omega) = \sum_{n=1}^{\infty} b_n \Psi_n(\mathbf{r}) \frac{\sigma_n}{1 + i\omega\sigma_n/\nu}, \tag{8a}$$

$$\tilde{p}(\mathbf{r}, \omega) = \sum_{n=1}^{\infty} b_n Q_n(\mathbf{r}) \frac{1}{1 + i\omega\sigma_n/\nu} + \Phi(\mathbf{r}). \tag{8b}$$

Here, the dimensionless vector eigenfunctions Ψ_n satisfy

$$-\nabla^2\Psi_n = \frac{1}{\sigma_n}(\Psi_n - \nabla Q_n), \tag{9a}$$

$$\nabla \cdot \Psi_n = 0, \tag{9b}$$

$$\Psi_n = 0, \text{ on the pore walls,} \tag{9c}$$

$$Q_n: \text{compact,} \tag{9d}$$

and the parameters σ_n , expressed in m^2 , are the inverse eigenvalues of the Stokes operator. They determine the viscous relaxation times $\Theta_n = \sigma_n/\nu$ corresponding to purely damped modes $\tilde{\mathbf{v}} = \sigma_n\Psi_n e^{-t/\Theta_n}$ as a solution to the homogeneous unsteady Stokes problem, i.e., with the external excitation term $\hat{\mathbf{g}} = 0$ in (5). The functions Q_n , which are non-zero in general, have dimensions of length and determine the corresponding compact pressures $\tilde{p} = Q_n e^{-t/\Theta_n}$. The largest value σ_1 is obviously of order $\mathcal{O}(a^2)$ and the parameters σ_n , sorted such that $\sigma_{n+1} < \sigma_n$, accumulate to 0 when $n \rightarrow \infty$. Using the conditions (9), it can be verified that the eigenfunctions Ψ are orthogonal. They are complete in the subspace of the square integrable divergence-free fields having a zero normal component on the pore walls. Furthermore, they are chosen orthonormal,

$$\frac{1}{V_f} \int_{V_f} \Psi_n \cdot \Psi_m dV = \delta_{nm}. \tag{10}$$

The dimensionless expansion coefficients b_n are defined as

$$b_n = \frac{1}{V_f} \int_{V_f} \Psi_n \cdot \mathbf{e} dV. \tag{11}$$

Now substituting (8a) and (8b) in the Stokes equation (7a) and using (9a), we see that (7a) is satisfied if

$$\sum_{n=1}^{\infty} b_n \Psi_n = \mathbf{e} - \nabla\Phi. \tag{12}$$

Note that there is a unique solution \mathbf{E}, Φ to the following electric problem:

$$\mathbf{E} = \mathbf{e} - \nabla\Phi, \tag{13a}$$

$$\nabla \cdot \mathbf{E} = 0, \tag{13b}$$

$$\mathbf{E} \cdot \mathbf{n} = 0, \text{ on the pore walls,} \tag{13c}$$

$$\Phi: \text{ compact,} \tag{13d}$$

where \mathbf{n} is the unit outward normal from the pore region. In particular, the identity $\sum_{n=1}^{\infty} b_n \Psi_n = \mathbf{E}$ holds. The field \mathbf{E} , which solves the corresponding electrical conduction problem for a porous medium filled with a conducting fluid and having an insulating solid phase, can be interpreted as the scaled electric field, i.e., the local electric field divided by the applied macroscopic potential gradient. Decomposition (13a) is referred to by Avellaneda and Torquato¹⁴ as the so-called Hodge decomposition. We notice that there is a direct relation to the tortuosity factor α_{∞} that determines the effective electric conductivity of the porous medium. Applying the unit electric field \mathbf{e} , the microscopic current in the saturating fluid is $\mathbf{j} = \sigma_f \mathbf{E}$, where σ_f is the fluid electric conductivity. The macroscopic current $\mathbf{J} = \phi \langle \mathbf{j} \rangle$ then obeys a macroscopic Ohm's law $\mathbf{J} = \sigma_{\text{eff}} \mathbf{e}$, with $\sigma_{\text{eff}} = \phi \sigma_f / \alpha_{\infty}$, and

$$\alpha_{\infty} = \frac{1}{\langle \mathbf{E} \rangle \cdot \mathbf{e}} = \frac{\langle \mathbf{E} \cdot \mathbf{E} \rangle}{\langle \mathbf{E} \rangle \cdot \langle \mathbf{E} \rangle}. \tag{14}$$

We assumed unidirectional or isotropic pore space so that the tortuosity is a scalar. After multiplying (12) by \mathbf{e} and averaging, the identity

$$\sum_{n=1}^{\infty} b_n^2 = \frac{1}{\alpha_{\infty}} \tag{15}$$

immediately follows.

On the macrolevel, Darcy's law describes the linear response of the macroscopic velocity $\hat{\mathbf{U}}$ to the source term $\hat{g}\mathbf{e}$:

$$\frac{\eta \phi}{k(\omega)} \hat{\mathbf{U}} = \hat{g}\mathbf{e}, \tag{16}$$

where $k(\omega)$ is the frequency-dependent, complex-valued dynamic permeability. This relation is the counterpart of the classical Darcy's law for steady-state flow, and reduces to it for $\omega \rightarrow 0$. In general, the dynamic permeability is a second-rank tensor that reduces to a scalar in the case of unidirectional, isotropic, or simple-cubic microstructures. In this case, the macroscopic flow $\hat{\mathbf{U}}$ is in the same direction as the source term $\hat{g}\mathbf{e}$, which means that $\hat{\mathbf{U}} = \langle \hat{\mathbf{v}} \cdot \mathbf{e} \rangle \mathbf{e}$. From (16), we now easily find that

$$\frac{k(\omega)}{\phi} = \langle \tilde{\mathbf{v}} \cdot \mathbf{e} \rangle. \tag{17}$$

Substitution of (8a) yields a series expansion for $k(\omega)$:

$$\frac{k(\omega)}{\phi} = \sum_{n=1}^{\infty} \frac{b_n^2 \sigma_n}{1 + i \omega \sigma_n / \nu}. \tag{18}$$

Another form of (17) is particularly useful. For any divergence-free vector field \mathbf{w} that has zero normal components on the interface, there is the identity

$$\langle \mathbf{w} \cdot \mathbf{e} \rangle = \langle \mathbf{w} \cdot \mathbf{E} \rangle, \tag{19}$$

which follows directly from (13a) after integrating by parts and using the compact character of the fields. Thus, we also have

$$\frac{k(\omega)}{\phi} = \langle \tilde{\mathbf{v}} \cdot \mathbf{E} \rangle. \tag{20}$$

The velocity response of the fluid to the source term $\hat{g}\mathbf{e}$ can also be defined in analogy with the response of an ideal fluid:

$$\rho_f \alpha(\omega) i \omega \hat{\mathbf{U}} = \hat{g}\mathbf{e}, \tag{21}$$

where $\alpha(\omega)$ is the frequency-dependent, complex-valued tortuosity,

$$\alpha(\omega) = \frac{\nu \phi}{i \omega k(\omega)}. \tag{22}$$

It may be verified that the following energetic representation of $\alpha(\omega)$ is valid:

$$\alpha(\omega) = \frac{\langle \tilde{\mathbf{v}} \cdot \tilde{\mathbf{v}}^* \rangle}{\langle \tilde{\mathbf{v}} \rangle \cdot \langle \tilde{\mathbf{v}}^* \rangle} - \frac{\nu}{i \omega} \frac{\langle \tilde{\mathbf{v}} \cdot \nabla^2 \tilde{\mathbf{v}}^* \rangle}{\langle \tilde{\mathbf{v}} \rangle \cdot \langle \tilde{\mathbf{v}}^* \rangle}, \tag{23}$$

where $*$ denotes complex conjugation. The proof is given in Appendix A. Using homogenization theory, this result was also obtained by Smeulders *et al.*³ Physically speaking, this result expresses the condition that the work performed by the external force per unit time is equal to the rate of change of the kinetic energy plus the dissipated energy per unit time. The real part of (23) is related to the kinetic energy, and the imaginary part is related to the mean rate of energy dissipation.

In the forthcoming, we will be mainly concerned with the high-frequency limit $\omega a^2 / \nu \rightarrow \infty$ of the dynamic permeability and tortuosity. In this limit, the denominators in (18) may be replaced by the factors $i \omega \sigma_n / \nu$ up to high values of n , thus showing that $k(\omega) \rightarrow \nu \phi / i \omega \alpha_{\infty}$, according to (15). Indeed, assuming that the viscous term $\nabla^2 \tilde{\mathbf{v}}$ is negligibly small compared to the inertial term in (7a), the Stokes problem (7) degenerates into the electric or ideal fluid problem (13), and $\tilde{\mathbf{v}} \rightarrow \mathbf{E} \nu / i \omega$. Substitution of this result for $\tilde{\mathbf{v}}$ in (17) or (20) again yields the above leading behavior of $k(\omega)$ at high frequencies, while substitution in (22) shows that the corresponding result for the dynamic tortuosity is $\alpha(\omega) \rightarrow \alpha_{\infty}$.

III. HIGH-FREQUENCY VELOCITY PATTERN IN SMOOTH GEOMETRIES

We now examine the precise limit of the Stokes problem (7) for $\varepsilon / a \rightarrow 0$, where ε is the complex viscous skin depth parameter,

$$\varepsilon = \sqrt{\nu / i \omega} = (1 - i) \delta / 2. \tag{24}$$

Writing the pressure \tilde{p} in the form $\tilde{p} = \tilde{q} + \Phi$ [see (8b)] and substituting in (7a), we get

$$\tilde{\mathbf{v}} = \varepsilon^2 (\mathbf{E} - \nabla \tilde{q} + \nabla^2 \tilde{\mathbf{v}}). \tag{25}$$

Taking the curl of (25), we obtain the diffusion equation for the vorticity, $\nabla \times \tilde{\mathbf{v}} - \varepsilon^2 \nabla^2 \nabla \times \tilde{\mathbf{v}} = 0$. Following Johnson *et al.*,⁴ we note that in the limit of high frequencies the viscous skin depth $\delta = 2|\varepsilon|$ eventually becomes much smaller

than any characteristic pore size a . Any vorticity generated at the pore walls decays to zero as one moves away distances of the order δ from the wall into the bulk of the pore. Thus, the Laplacian $\nabla^2 \tilde{\mathbf{v}} = -\nabla \times \nabla \times \tilde{\mathbf{v}}$, vanishes in the bulk fluid, except for a boundary layer of thickness δ near the pore walls. It follows that outside this boundary layer, the fluid motion is that of potential flow, with

$$\tilde{\mathbf{v}} = \tilde{\mathbf{v}}_p = \varepsilon^2 (\mathbf{E} - \nabla \tilde{q}). \tag{26}$$

It will be seen below that the presence of the pressure gradient term $-\nabla \tilde{q}$ is a small $\mathcal{O}(\varepsilon/a)$ correction to the leading $\mathcal{O}(1)$ flow pattern \mathbf{E} that appears because small *normal components* of the velocity are created at the virtual interface between the bulk potential flow region and the viscous boundary layer. Clearly, such normal components would not exist in straight channels for obvious symmetry reasons, and must therefore be related to the curvature of the pore walls. The *tangential* components of the velocity in the boundary layer can be directly evaluated to leading order in terms of the \mathbf{E} field only. Indeed, since δ is arbitrary small at high enough frequencies, the walls of the pore appear to be flat in the region where the tangential velocity goes from 0 at the pore wall to the value $\varepsilon^2 \mathbf{E}$ in the pore region. Thus, the tangential components of the velocity may be written to leading order,¹⁵

$$\tilde{\mathbf{v}} = \varepsilon^2 \mathbf{E}(\mathbf{r}_w) (1 - e^{-\beta/\varepsilon}), \tag{27}$$

where β is a local coordinate measured from the pore wall at position \mathbf{r}_w into the bulk of the pore: $\mathbf{r} - \mathbf{r}_w = -\beta \mathbf{n}$. Since \mathbf{E} varies at the pore scale $a \gg \delta$, no distinction is to be made between \mathbf{r} and \mathbf{r}_w in (27). Thus, we may combine (26) and (27) and consider the velocity field $\tilde{\mathbf{v}}$, including leading-order tangential and normal components, as the solution of the problem,

$$\tilde{\mathbf{v}} = \sigma(\mathbf{r})(\mathbf{E} - \nabla \Pi), \tag{28a}$$

$$\nabla \cdot \tilde{\mathbf{v}} = 0, \tag{28b}$$

$$\sigma(\mathbf{r}) = \varepsilon^2 (1 - e^{-\beta/\varepsilon}), \tag{28c}$$

where we have introduced a compact field Π , which is related to \tilde{q} and defined as

$$\nabla \Pi = (1 - e^{-\beta/\varepsilon})^{-1} \nabla \tilde{q}, \tag{29a}$$

in the boundary layer, and

$$\nabla \Pi = \nabla \tilde{q}, \tag{29b}$$

outside. The field $\tilde{\mathbf{v}}$ then solves the electrical conduction problem for a porous medium having an insulating solid phase and filled with a conducting fluid of conductivity $\sigma(\mathbf{r})$. Current conservation gives

$$-\nabla \cdot (\sigma \nabla \Pi) + \mathbf{E} \cdot \nabla \sigma = 0. \tag{30}$$

In the limit $\varepsilon/a \rightarrow 0$, only derivatives normal to the pore walls need to be considered in the boundary layer and it is convenient to introduce the stretched coordinate $\zeta = \beta/\varepsilon$ to express the fact that σ is a function of ζ only. In addition, the normal component of the unperturbed electric field E_β ,

which varies at scale a and is zero on the pore walls, may be replaced by its first-order term $\varepsilon \zeta (\partial E_\beta / \partial \beta)_{\beta=0}$. Equation (30) is easily integrated to yield

$$\frac{\partial \Pi}{\partial \beta} = \varepsilon \left(\frac{1 - (1 + \zeta) e^{-\zeta}}{1 - e^{-\zeta}} \right) \left(\frac{\partial E_\beta}{\partial \beta} \right)_{\beta=0}. \tag{31}$$

We conclude that outside the boundary layer, the perturbed electric field is of the form

$$-\nabla \Pi = \varepsilon \mathbf{N}, \tag{32}$$

where \mathbf{N} is the unique solution of the problem:

$$\mathbf{N}: \text{ gradient of a compact field,} \tag{33a}$$

$$\nabla \cdot \mathbf{N} = 0, \tag{33b}$$

$$\mathbf{N} \cdot \mathbf{n} = \left(\frac{\partial E_\beta}{\partial \beta} \right)_{\beta=0}, \text{ on the pore walls.} \tag{33c}$$

We note that since Π is a compact field, the perturbed field $\varepsilon \mathbf{N}$ is orthogonal to \mathbf{E} in an averaged sense:

$$\langle \mathbf{E} \cdot \mathbf{N} \rangle = 0. \tag{34}$$

This can be seen from the same reasoning used to obtain (19): because \mathbf{E} is divergence-free and has zero normal components on the interface, (34) follows after integrating by parts and using the compact character of the fields. Explicit expressions for the velocity fields inside and outside the boundary layer result immediately. Inside the boundary layer we find, using (28a), (28c), and (31)

$$\begin{aligned} \tilde{\mathbf{v}} = & \varepsilon^2 (1 - e^{-\beta/\varepsilon}) \mathbf{E}(\mathbf{r}_w) + \varepsilon^3 \left[1 - \left(1 + \frac{\beta}{\varepsilon} \right) e^{-\beta/\varepsilon} \right] \\ & \times \left(\frac{\partial E_\beta}{\partial \beta} \right)_{\beta=0} \mathbf{n}, \end{aligned} \tag{35a}$$

and outside the boundary layer we have, using (26), (29b), and (32)

$$\tilde{\mathbf{v}} = \varepsilon^2 [\mathbf{E}(\mathbf{r}) + \varepsilon \mathbf{N}(\mathbf{r})]. \tag{35b}$$

As mentioned previously, small normal components of the velocity are induced in the boundary layer, and these act as a source for the additional ideal fluid flow $\varepsilon^3 \mathbf{N}$ in the bulk. Note that, though \mathbf{N} is an ideal fluid flow, it is related to the viscous nature of the fluid. This flow is orthogonal to the main flow $\varepsilon^2 \mathbf{E}$, and has nonvanishing mean value. This precise representation of the velocity pattern, which, however, does not include higher-order boundary layer tangential terms $\mathcal{O}(\varepsilon^3/a)$ in (35a) and higher-order bulk terms $\mathcal{O}(\varepsilon^4/a^2)$ in (35b), is used in the next section to clarify the algebra involved in the high-frequency behavior of the dynamic permeability and tortuosity.

IV. HIGH-FREQUENCY PERMEABILITY AND TORTUOSITY

As suggested in the previous section by the analysis of the velocity field for materials with bounded curvature of the pore surface interface, the high-frequency development of the dynamic permeability and tortuosity may be written in successive powers of the viscous skin depth parameter:

$$\alpha(\omega) = \alpha_\infty(1 + C\varepsilon + D\varepsilon^2 + \dots), \tag{36a}$$

$$\frac{k(\omega)}{\phi} = \frac{\varepsilon^2}{\alpha_\infty} [1 - C\varepsilon + (C^2 - D)\varepsilon^2 + \dots]. \tag{36b}$$

Three equivalent determinations of the C parameter will now be considered, using either (17), (20), or (23). The first is a new derivation that supplements in the proper manner the incomplete determination by Sheng and Zhou.⁵ The second is equivalent to the original arguments by Johnson *et al.*,⁴ and the third was employed by Avellaneda and Torquato,¹⁴ though they did not capture all the details involved. The third method is the simplest one, and will also be applied in Sec. VI to capture some of the effects related to the presence of sharp edges in the pore wall geometry. We will show that in that case the set of equations (36) is modified as follows:

$$\alpha(\omega) = \alpha_\infty(1 + C\varepsilon + C_1\varepsilon^w + \dots), \tag{37a}$$

$$\frac{k(\omega)}{\phi} = \frac{\varepsilon^2}{\alpha_\infty} (1 - C\varepsilon - C_1\varepsilon^w + \dots), \tag{37b}$$

with the same inverse length C as before and the exponent w ($1 < w < 2$) related to the apex angle of the edges.

To proceed now in the most direct manner, we substitute (35a) and (35b) into (17). Integrating the velocity field in the whole fluid volume, we have

$$\int_{V_f} \tilde{\mathbf{v}} \cdot \mathbf{e} dV = \varepsilon^2 \int_{V_f} \mathbf{E} \cdot \mathbf{e} dV - \varepsilon^2 \int_{BL} e^{-\beta/\varepsilon} \mathbf{E} \cdot \mathbf{e} dV + \varepsilon^3 \int_{IF} \mathbf{N} \cdot \mathbf{e} dV, \tag{38}$$

where the subscripts BL and IF denote integration over the boundary layer and the ideal fluid region, respectively. Note that we have not written the negligible contribution of the normal components of the velocity in the boundary layer. Such a contribution would be associated with the constant D in (36a) and (36b) and is meaningless due to the higher-order tangential terms $\mathcal{O}(\varepsilon^3/a)$ not written in (35a) and the higher-order bulk terms $\mathcal{O}(\varepsilon^4/a^2)$ not written in (35b). The boundary layer contribution reduces exactly to a boundary integral $-\varepsilon^3 \int_{S_p} \mathbf{E} \cdot \mathbf{e} dS$ that is performed on the boundary walls. Moreover, extending with negligible error the volume of integration in the last term of (38) to be that of the whole fluid, and using the orthogonality property (34), this last term is written as $\varepsilon^3 \int_{V_f} \nabla \Phi \cdot \mathbf{N} dV$. Integrating by parts, it can also be written as a boundary integral on the pore walls, namely $\varepsilon^3 \int_{S_p} \Phi \mathbf{N} \cdot \mathbf{n} dS$. We thus obtain the result

$$\frac{k(\omega)}{\phi} = \frac{\varepsilon^2}{\alpha_\infty} (1 - C\varepsilon + \dots), \tag{39}$$

with

$$C = \frac{\alpha_\infty}{V_f} \int_{S_p} \left(\mathbf{E} \cdot \mathbf{e} - \Phi \frac{\partial E_\beta}{\partial \beta} \right) dS = \int_{S_p} \left(\mathbf{E} \cdot \mathbf{e} - \Phi \frac{\partial E_\beta}{\partial \beta} \right) dS \Big/ \int_{V_f} \mathbf{E}^2 dV. \tag{40}$$

This is an important result, which allows us to compare earlier results from literature. As it holds that

$$\int_{S_p} \Phi \frac{\partial \mathbf{E}_\beta}{\partial \beta} dS = \int_{S_p} \mathbf{E} \cdot \nabla \Phi dS \tag{41}$$

(see Appendix B), we may write that

$$C = \frac{2}{\Lambda} = \frac{\int_{S_p} \mathbf{E}^2 dS}{\int_{V_f} \mathbf{E}^2 dV}, \tag{42}$$

where we have used (13a). This is the classical expression of Johnson *et al.*,⁴ who were the first to define the length-scale parameter Λ as the weighted pore volume (V_f)-to-pore surface (S_p) ratio. For tube flow, Λ equals the tube radius.

Equation (42) can also be obtained using the following energetic arguments. From (36a) we derive that, to the leading order in the high-frequency limit,

$$\frac{\text{Im } \alpha(\omega)}{\text{Re } \alpha(\omega)} = -C \frac{\delta}{2}. \tag{43}$$

On the other hand, from (23), we have that

$$\frac{\text{Im } \alpha(\omega)}{\text{Re } \alpha(\omega)} = \frac{\delta^2 \langle \tilde{\mathbf{v}} \cdot \nabla^2 \tilde{\mathbf{v}}^* \rangle}{2 \langle \tilde{\mathbf{v}} \cdot \tilde{\mathbf{v}}^* \rangle}. \tag{44}$$

This means that we may write

$$C = \lim_{\delta/a \rightarrow 0} \delta \frac{\langle \tilde{\mathbf{v}} \cdot \nabla^2 \tilde{\mathbf{v}}^* \rangle}{\langle \tilde{\mathbf{v}} \cdot \tilde{\mathbf{v}}^* \rangle}. \tag{45}$$

Substituting $\tilde{\mathbf{v}} \approx \tilde{\mathbf{v}}^* \approx \mathbf{E}$, and $\nabla^2 \tilde{\mathbf{v}}^* \approx -\mathbf{E} e^{-\beta/\varepsilon^*}$ [see (27)], and performing the integrals immediately yields (42). Note that because of the Laplacian in the numerator, there is no integration in the bulk but only a boundary layer contribution. Note also that there is no first-order contribution of the perturbed potential flow $\varepsilon \mathbf{N}$ to the denominator due to the orthogonality with the unperturbed flow \mathbf{E} .

Finally, another method to obtain (42) is to use (20). From (36b) we have that

$$\lim_{\delta/a \rightarrow 0} \frac{\text{Re } k(\omega)}{\phi} = \frac{1}{\sqrt{2}} \frac{C}{\alpha_\infty} \left(\frac{\nu}{\omega} \right)^{3/2} = \frac{\sqrt{2}}{\Lambda \alpha_\infty} \left(\frac{\nu}{\omega} \right)^{3/2}. \tag{46}$$

Thus, from (20) it follows that

$$C = \lim_{\delta/a \rightarrow 0} \sqrt{2} \alpha_\infty \left(\frac{\omega}{\nu} \right)^{3/2} \text{Re} \langle \tilde{\mathbf{v}} \cdot \mathbf{E} \rangle. \tag{47}$$

Now, substituting the velocity pattern (35), there is no bulk contribution from the perturbed potential flow $\varepsilon^3 \mathbf{N}$ that is orthogonal to \mathbf{E} . There is also no bulk contribution from the unperturbed leading-order term $\varepsilon^2 \mathbf{E}$ that is purely imaginary. There is only a simple boundary layer contribution to evaluate, which again leads to (42).

In literature other expressions for Λ can be found. The expression obtained by Sheng and Zhou⁵ and Zhou and Sheng⁶ was as follows:

$$\frac{2}{\Lambda} = \frac{\int_{S_p} \mathbf{E} \cdot \mathbf{e} dS}{\int_{V_f} \mathbf{E}^2 dV}. \tag{48}$$

We notice that this is only the first term in (40). The origin of the incompleteness is the use of the “linear” average (17) without taking into account the bulk contribution from the small perturbed potential field $\varepsilon^3\mathbf{N}$. The same expression (48) can be found in Pride¹⁶ in the context of electrokinetic effects for sound propagation in a porous medium saturated with a conductive fluid. Avellaneda and Torquato¹⁴ tried to clarify the discrepancy between (42) and (48) by considering higher-order terms in the boundary layer calculation suggested by Sheng and Zhou.⁵ However, the missing contribution is a bulk term and their boundary layer analysis was still incomplete.

To illustrate our dynamic permeability analysis, we will first consider two straightforward models for porous media that are wellknown in literature. Next, the effect of the perturbed bulk contribution will be demonstrated in the case of corrugated pore channels.

V. NONCORRUGATED PORE CHANNELS

As a model for porous media, Biot¹⁷ discussed an ensemble of parallel identical cylindrical tubes within a solid. The tube radius is R . The number density of tubes is represented by the porosity ϕ . When the fluid flow is oriented along the cylinder axis of the tubes, it was already shown by Zwikker and Kosten¹⁸ that

$$\tilde{k}(\omega) = \frac{k(\omega)}{k_0} = \frac{8}{i\kappa^2} \left(1 - \frac{2J_1(i^{3/2}\kappa)}{i^{3/2}\kappa J_0(i^{3/2}\kappa)} \right), \quad (49)$$

where $\kappa = R\sqrt{\omega/\nu}$ is the so-called Womersley number, and J_0 and J_1 are Bessel functions of the zeroth and first order. Poiseuille flow prescribes that $k_0 = \frac{1}{8}\phi R^2$. This means that the characteristic frequency $\omega_c = \nu\phi/k_0\alpha_\infty$ is equal to $8\nu/R^2$ in this case, and $\kappa = \sqrt{8\omega/\omega_c}$. For high frequencies, it follows directly from (49) that¹⁷

$$\lim_{\omega \rightarrow \infty} \tilde{k} = \frac{1}{i\tilde{\omega}} \left(1 - \frac{1-i}{2\sqrt{\tilde{\omega}}} \right), \quad (50)$$

where we have introduced $\tilde{\omega} = \omega/\omega_c$. This expression is in agreement with (46), which is most conveniently shown by writing (46) as $\lim_{\omega \rightarrow \infty} \tilde{k} = \frac{1}{2}\sqrt{M}\tilde{\omega}^{-3/2}$, where M is the so-called shape factor:

$$M = 8k_0\alpha_\infty/\phi\Lambda^2 = 8Fk_0/\Lambda^2, \quad (51)$$

which is identical to 1 in this case.

Another model that was discussed by Biot¹⁷ consists of an ensemble of identical two-dimensional slits (slit opening $2R$) within a solid. When the flow is oriented along the slit layers, it can be shown that

$$\tilde{k}(\omega) = \frac{3}{i\kappa^2} \left(1 - \frac{\tanh(i^{1/2}\kappa)}{i^{1/2}\kappa} \right). \quad (52)$$

Here we find that $k_0 = \frac{1}{3}\phi R^2$, so that for this configuration $\omega_c = 3\nu/R^2$, and $\kappa = \sqrt{3\omega/\omega_c}$. The high-frequency limit is now given by

$$\lim_{\omega \rightarrow \infty} \tilde{k} = \frac{1}{i\tilde{\omega}} \left(1 - \frac{1-i}{\sqrt{6\tilde{\omega}}} \right). \quad (53)$$

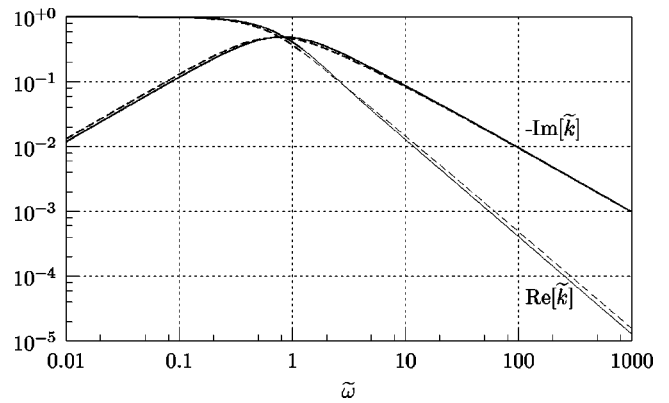


FIG. 1. Dynamic permeability for tube flow (dashed line) and slit flow (solid line).

Also, this expression is in agreement with (46), because for slit flow $M = \frac{2}{3}$. The real and imaginary parts of the dynamic permeability for both the tube model and the slit model are plotted in Fig. 1. We notice that there are only minor differences between both models. For low frequencies, the real part of the dynamic permeability approaches the stationary Darcy permeability, whereas the imaginary part tends to zero. For high frequencies, the imaginary part of the dynamic permeability shows a $-1/\tilde{\omega}$ dependency for both the tube and the slit model, whereas for the real part the $\tilde{\omega}^{-3/2}$ behavior can be discerned. We also notice that the rollover from low-frequency viscous behavior to high-frequency inertia behavior is observed at $\omega \approx \omega_c$ indeed.

VI. CORRUGATED PORE CHANNELS

We noticed in Sec. IV that the bulk contribution from the small perturbed field $\varepsilon^3\mathbf{N}$ has to be taken into account in order to describe correctly the velocity field for materials with bounded curvature of the pore surface interface. The effect of this contribution can elegantly be illustrated in the case of corrugated pore channels, where we will show that the use of (17) instead of (20) yields erroneous predictions for w in (37a) and (37b). We will therefore investigate the influence of wedge-shaped surface asperities on high-frequency permeability. The two-dimensional periodic geometry considered is depicted in Fig. 2. The wedge is defined by its apex angle γ . Introducing cylindrical coordinates r, θ , we set the origin $r=0$ on the apex P_3 of the wedge and count the angle θ from one side of the wedge. The singular potential field $\mathbf{E}(r, \theta)$ is given by¹⁵

$$E_r = Anr^{n-1} \cos n\theta, \quad (54)$$

$$E_\theta = -Anr^{n-1} \sin n\theta, \quad (55)$$

where A is an amplitude factor and $\frac{1}{2} < n = \pi/(2\pi - \gamma) < 1$. Introducing the dimensionless stretched boundary layer variable $\rho = r/\varepsilon$, we find that

$$E_r = An\varepsilon^{n-1}\rho^{n-1} \cos n\theta = \mathcal{O}(\varepsilon^{n-1}), \quad (56)$$

$$E_\theta = -An\varepsilon^{n-1}\rho^{n-1} \sin n\theta = \mathcal{O}(\varepsilon^{n-1}). \quad (57)$$

To evaluate the high-frequency limit of the permeability, we will consider the limit of the real part of (20):

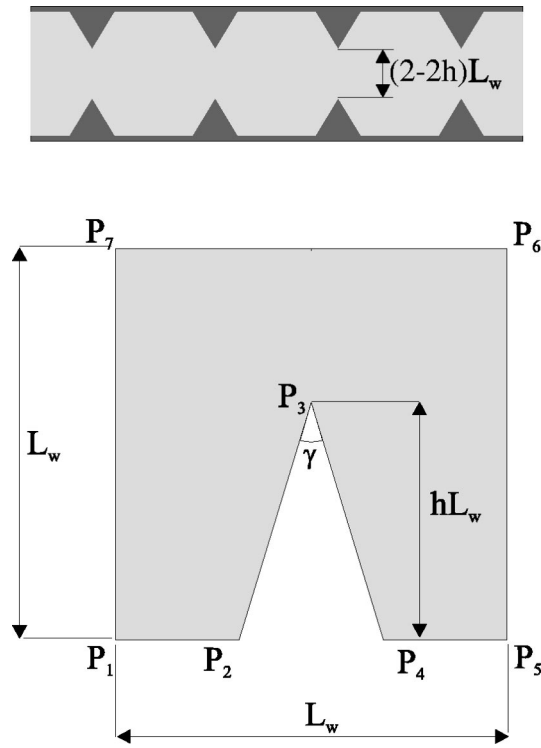


FIG. 2. Geometry of two-dimensional pore channel (top) and of the periodic cell (bottom).

$$\lim_{\varepsilon/a \rightarrow 0} \frac{\text{Re } k(\omega)}{\phi} = \lim_{\varepsilon/a \rightarrow 0} \text{Re}(\tilde{\mathbf{v}} \cdot \mathbf{E}). \quad (58)$$

The integral may be split in the bulk fluid contribution from the potential flow region and the boundary layer contribution. The general argument leading to the decomposition (26) in the bulk fluid was not concerned with any detailed calculation of what actually happens in the boundary layer. Similarly, the orthogonality property $-\langle \mathbf{E} \cdot \nabla \tilde{q} \rangle = 0$ between the “ground state” field \mathbf{E} and the perturbed field $-\nabla \tilde{q}$ is essentially due to the compact character of the pressure field \tilde{q} and is not concerned with the specific distribution of this field. This is why there is, as before, no contribution to (58) from the potential flow region. We only have to evaluate the boundary layer contribution. The boundary layer may be divided in two different parts. “Far” from the tip of the wedges, the boundary layer will have the usual flat-surface profile. “Near” the tip of the wedges, the boundary layer profile will be significantly different from the flat-surface profile. The pertinent length scale giving these notions of “far” and “near” is obviously the diffusion length of the vorticity, i.e., the viscous skin depth $\delta = \sqrt{2\nu/\omega}$. Let L_w be the separation between the tips of the wedges along the pore surface (see Fig. 2). Clearly, as δ/L_w goes to zero, the region of extent δ along the pore surface where the boundary layer is of the nonplane “near”-type is small compared to the region of extent L_w , where the boundary layer has the usual flat-surface profile. As will be verified below, the leading correction $-C\varepsilon$ in the developments (36) is not affected. Here we assumed that the apex angle γ is strictly larger than zero, so that the Johnson *et al.*⁴ Λ parameter remains defined.

The contributions of the wedges to (58) due to the nonplane “near”-type boundary layers is now shown to produce correction terms between the second and the third term in (36), as indicated in (37).

We consider Stokes equation (25),

$$\tilde{\mathbf{v}} - \varepsilon^2 \nabla^2 \tilde{\mathbf{v}} = \varepsilon^2 (\mathbf{E} - \nabla \tilde{q}), \quad (59)$$

in the “near”-region around the tip. In the flat-surface case, the gradient $-\nabla \tilde{q}$ was a small correction with an extra factor ε compared to \mathbf{E} . The pressure gradient term $-\nabla \tilde{q}$ describes the modification of the inertial solid–fluid reaction force due to the viscous effects. Its averaged value $\langle -\nabla \tilde{q} \rangle$ will be smaller, in magnitude, than the external unit force \mathbf{e} . Thus, using the estimate (56)–(57) we may conclude that, to the leading order, $\tilde{\mathbf{v}} = \mathcal{O}(\varepsilon^{n+1})$. Now performing the integral in (58) around the tip of the wedge, we find that

$$\begin{aligned} \text{Re} \int_0^\beta \int_0^{\theta_0} \tilde{\mathbf{v}} \cdot \mathbf{E} dV &= \text{Re} \left(\varepsilon^2 \int_0^{\beta/\varepsilon} \int_0^{\theta_0} \tilde{\mathbf{v}} \cdot \mathbf{E} \rho d\theta d\rho \right) \\ &= \text{Re}[\varepsilon^2 \mathcal{O}(\varepsilon^{2n})] = \text{Re} \mathcal{O}(\varepsilon^{2n+2}). \end{aligned} \quad (60)$$

From (58) and (60) we thus find that

$$\lim_{\varepsilon/a \rightarrow 0} \frac{\text{Re } k(\omega)}{\phi} = \text{Re} \mathcal{O}(\varepsilon^{2n+2}). \quad (61)$$

Comparing with (37b) yields that

$$w = 2n = \frac{2\pi}{2\pi - \gamma}. \quad (62)$$

In a paper by Achdou and Avellaneda,¹³ an analogous reasoning was followed for the problem of corrugated pore channels. However, they did not multiply the velocity field $\tilde{\mathbf{v}}$ by the electric field \mathbf{E} in (60), thus obtaining an $\mathcal{O}(\varepsilon^{n+3})$ dependence leading to $w = n + 1$ [see Achdou and Avellaneda,¹³ Eq. (E7)]. However, when the linear average (17) is employed, it is not possible to evaluate the high-frequency limit of the permeability by only considering what happens in the boundary layer. There is a missing contribution from the perturbed potential flow in the bulk. The significant difference between (60) and the Achdou and Avellaneda¹³ result shows that in the case of wedges the bulk contribution dominates the boundary layer contribution, whereas in the bounded curvature case both contributions were of the same order. These findings will now be substantiated numerically.

VII. NUMERICAL COMPUTATIONS

Numerical computations were performed on the periodic polygon $P_1 \cdots P_7$, depicted in Fig. 2. The periodic cell $P_1 P_5 P_6 P_7$ is a square with sides L_w . The apex angle of the wedge is γ , and its height is hL_w , thus leaving a channel opening $(2-2h)L_w$ (see Fig. 2). Numerical results are presented for varying γ where h is set 0.5, and for varying h , where $\tan \gamma/2$ is set 0.5. Taking the pressure gradient in the horizontal direction, the Stokes problem (7) was solved using a finite-element code based on a Uzawa decomposition method. A Dirichlet-type boundary condition was prescribed at the pore walls: $\tilde{\mathbf{v}} = 0$. The solution to the Stokes problem is

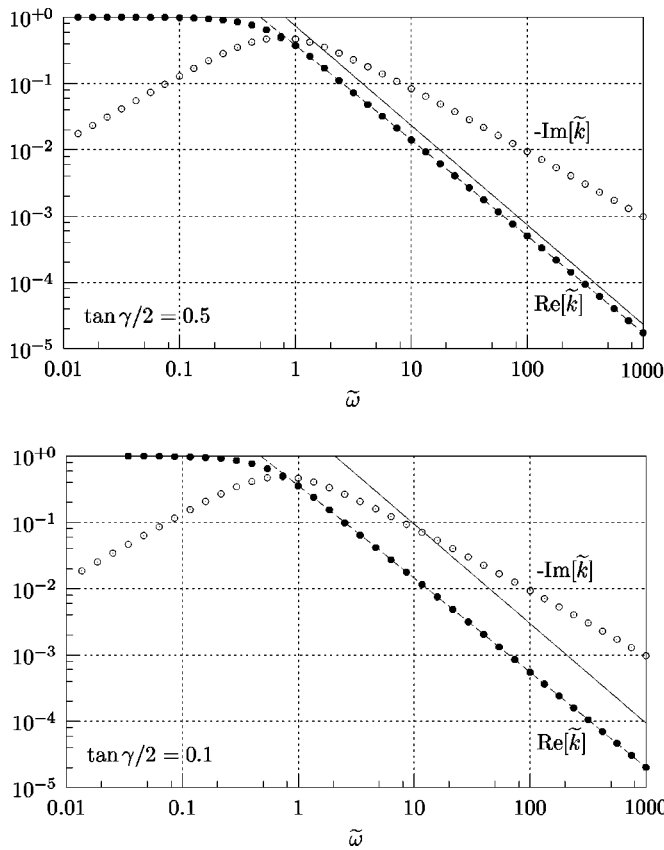


FIG. 3. Real and imaginary parts of the dynamic permeability for $\tan \gamma/2 = 0.5$ (top), and $\tan \gamma/2 = 0.1$ (bottom). In both figures $h = 0.5$. The circles and dots represent the numerical results. Both classical (solid lines) and improved (dashed lines) high-frequency approximations for $\text{Re}[\tilde{k}]$ are plotted.

approximated by means of N_1 finite elements and by using the variational formulation of the problem. To ensure accuracy, we have used an iterative automatic method, i.e., the solution is computed on the N_1 mesh, next an *a posteriori* estimate of the error is computed, and finally the mesh is locally refined accordingly by means of a Delaunay technique developed by Rebay.²⁰ Successful use of this refinement method on sharp-edged wedges was reported by Firdaouss *et al.*¹¹ Once the flow field is known, the dynamic permeability is computed using (17).

Two typical results are shown in Fig. 3, where the real and imaginary parts of the dynamic permeability are plotted for $\tan \gamma/2 = 0.5$ and for $\tan \gamma/2 = 0.1$. In both cases, $h = 0.5$. The high-frequency approximation $\frac{1}{2}\sqrt{M}\tilde{\omega}^{-3/2}$ is drawn as straight lines in both plots. An improved high-frequency approximation is also drawn (dashed line), which will be discussed hereafter. The parameters M and ω_c were computed independently, as discussed by Cortis and Smeulders.¹² We notice that for both apex angles the $-1/\tilde{\omega}$ dependency for the imaginary part of the dynamic permeability is preserved for high frequencies. For the real part of the dynamic permeability, however, significant departures from the predicted $\frac{1}{2}\sqrt{M}\tilde{\omega}^{-3/2}$ behavior are found. Apparently, these discrepancies become more significant for smaller apex angle, i.e., for sharper edges (see Fig. 3). These

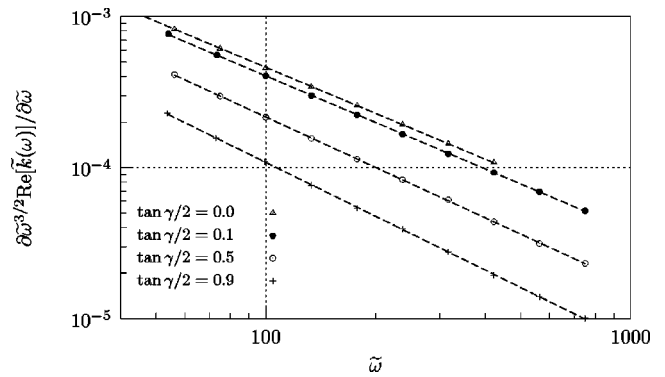


FIG. 4. Regression lines to determine the exponent w .

findings are in agreement with those of Achdou and Avellaneda,¹³ who reported that the presence of a wedge in the flow channel induces a nonanalytic dependence on the viscous skin depth $\delta = \sqrt{2\nu/\omega}$, and a slower convergence of $\tilde{k}(\omega)$ to its asymptotic limit than predicted by (46). They subsequently argue that the high-frequency behavior should be described as the combination of the asymptotic expansion (46) for laminar boundary layers and the contribution of the singularity as described by (37b):

$$\lim_{\omega \rightarrow \infty} \text{Re} \tilde{k}(\omega) = \frac{1}{2} \sqrt{M} \tilde{\omega}^{-3/2} [1 + C_1 \tilde{\omega}^{(1/2)(1-w)}], \quad (63)$$

or alternatively,

$$\lim_{\omega \rightarrow \infty} \tilde{\omega}^{3/2} \text{Re} \tilde{k}(\omega) = \frac{1}{2} \sqrt{M} + \frac{1}{2} C_1 \tilde{\omega}^{(1/2)(1-w)} \sqrt{M}, \quad (64)$$

where C_1 is a numerical constant and the exponent w is related to the wedge angle γ . The shape factor M is defined in (51). In Sec. VI it is derived that $w = 2n = 2\pi/(2\pi - \gamma)$ [see (62)], whereas Achdou and Avellaneda¹³ arrived at $w = 1 + n = (3\pi - \gamma)/(2\pi - \gamma)$. We notice that for $C_1 = 0$, we find back the asymptotic behavior (46). Our numerical computations now offer the possibility of determining the values of w and also M independently. In Fig. 4, we plotted the derivative $\partial[\tilde{\omega}^{3/2} \text{Re} \tilde{k}(\omega)]/\partial \tilde{\omega}$ against $\tilde{\omega}$ on a double logarithmic scale for various apex angles γ . This derivative was computed by means of a three-point centered finite difference method. We notice that for high frequencies, these curves become straight lines, which is in agreement with (64). Linear regression now yields the slope $\frac{1}{2}(1-w) - 1$ of the curve, and the value $\frac{1}{2}C_1(1-w)\sqrt{M}$. Consequently, the value of $\frac{1}{2}C_1\sqrt{M}$ in (64) is also known, and M can be obtained from linear regression of $\tilde{\omega}^{3/2} \text{Re} \tilde{k}(\omega)$ vs $\tilde{\omega}^{(1/2)(1-w)}$. The results are given in Table I, and Figs. 5 and 6.

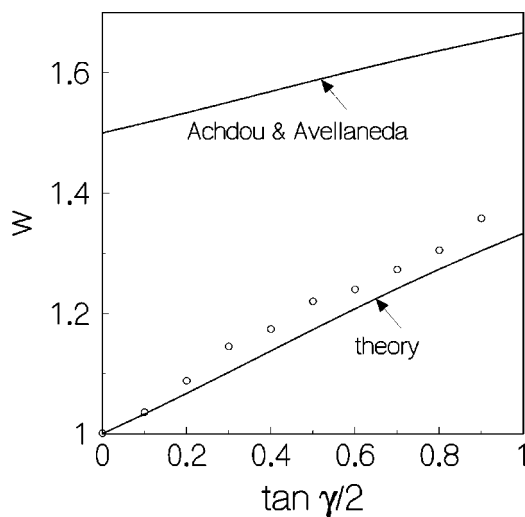
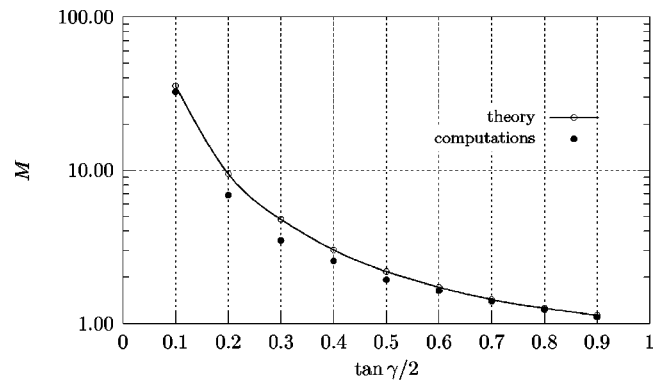
We notice that the present theory is only slightly underestimating the numerical results for w , whereas the Achdou and Avellaneda¹³ predictions give a considerable overestimation of the computations. Also in the limiting case of knife-edge singularities ($\gamma = 0$), there is a good agreement between the computations and the present theory. We also notice that the M values are reasonably close to the theoretical value $M = 8Fk_0/\Lambda^2$. This suggests that this definition for M is also correct in the case of surface roughness, and

TABLE I. Dependencies of the exponent w and the scaling parameter M on the wedge apex angle γ for constant $h=0.5$.

tan $\gamma/2$	w			M	
	Computations	Theory	Achdou and Avellaneda	Computations	Theory
0.0	1.001	1.000	1.500	992.74	∞
0.1	1.036	1.033	1.516	32.42	35.412
0.2	1.088	1.067	1.534	6.86	9.461
0.3	1.145	1.102	1.551	3.47	4.765
0.4	1.174	1.138	1.569	2.55	3.012
0.5	1.220	1.173	1.587	1.92	2.182
0.6	1.240	1.208	1.604	1.62	1.722
0.7	1.273	1.241	1.621	1.39	1.430
0.8	1.305	1.274	1.637	1.22	1.254
0.9	1.358	1.304	1.652	1.09	1.131

that the contribution of the singularities can indeed be captured in a nonanalytic extension of the existing theory without affecting the parameters of such theory. The obtained results for w and M are substituted in the high-frequency correction (63), which is plotted in Fig. 3. As expected, we find excellent agreement.

The effect of the channel opening was checked by varying the intrusion height h , while keeping $\tan \gamma/2=0.5$. Obviously this should not affect the value for w , which only depends on the apex angle γ . From (62) we find that the theoretical value is 1.173. The computations are summarized in Table II. We notice that for small wedge heights, the computations deviate from theory, because the effect of the flat wall is predominant over the effect of the singularity. On the other hand, for very small openings, the results also deviate from theory since the presence of the opposite wedge disturbs the flow field with respect to the assumptions made in Sec. VI. We notice that good results are obtained for $h=0.5$, which is the value we used for the computations in Table I.

FIG. 5. Dependence of the exponent w on the wedge apex angle γ for $h=0.5$. The circles represent the numerical computations.FIG. 6. Dependence of the shape factor M on the wedge apex angle γ for $h=0.5$.

VIII. CONCLUSIONS

We analyzed in detail the high-frequency fluid velocity patterns in the bulk fluid and the boundary layer for smooth and corrugated geometries. The classical Johnson *et al.*⁴ high-frequency limit for smooth geometries was obtained in different manners, thus clarifying the discrepancy with the Sheng and Zhou⁵ treatment and the Torquato¹⁴ approach. Two different contributions to the dynamic permeability are now apparent. One comes from the boundary layer near the pore walls; another comes from a perturbed potential flow in the bulk, induced in a nontrivial geometry by the presence of the boundary layer. This understanding has been applied to derive the correct form of the leading higher-order terms that are present in corrugated pore channels. Such terms are essential to obtain the correct high-frequency behavior of the dynamic permeability when sharp edges are present. In such cases the bulk contribution dominates the contribution from the boundary layer, which causes a slower convergence of $k(\omega)$ to its asymptotic limit than predicted from the classical theory by Johnson *et al.*⁴ We numerically investigated the dependency of the high-frequency behavior on the wedge angle in corrugated channels. For various angles, we computed the dynamic permeability by means of a precise finite element solver for the Stokes' flow. The effect of varying channel opening was investigated separately. The form of the leading higher-order terms was validated by our numerical results. Moreover, we found that the contribution of the wedge singularities does not affect the original parameters of the Johnson *et al.*⁴ theory.

TABLE II. Dependence of the exponent w on the wedge height h for constant γ ($\tan \gamma/2=0.5$). The theoretical value is 1.173.

h	w
	Computations
0.1	1.430
0.2	1.347
0.3	1.216
0.4	1.235
0.5	1.220
0.6	1.241
0.7	1.267

APPENDIX A: ENERGETIC REPRESENTATION OF THE DYNAMIC TORTUOSITY

Here we derive the relation (23) using the eigenmode formalism. First we define the notation:

$$\tilde{\sigma}_n = \frac{\sigma_n}{1 + i\omega\sigma_n/\nu}, \tag{A1}$$

and the mean symbol

$$\|X_n\| = \sum_{n=1}^{\infty} b_n^2 X_n. \tag{A2}$$

Then (18) and (22) read as

$$\frac{k(\omega)}{\phi} = \|\tilde{\sigma}_n\|, \tag{A3}$$

and

$$\alpha(\omega) = \frac{\nu}{i\omega\|\tilde{\sigma}_n\|}. \tag{A4}$$

From (A4) we write

$$\alpha(\omega) = \frac{\nu}{i\omega} \frac{\|\tilde{\sigma}_n^*\|}{\|\tilde{\sigma}_n\|\|\tilde{\sigma}_n^*\|}, \tag{A5}$$

where * denotes complex conjugation. Combining (A5) with the identity

$$\|\tilde{\sigma}_n^*\| = \frac{i\omega}{\nu} \|\tilde{\sigma}_n\tilde{\sigma}_n^*\| + \|\tilde{\sigma}_n\tilde{\sigma}_n^*/\sigma_n\|, \tag{A6}$$

we get

$$\alpha(\omega) = \frac{\|\tilde{\sigma}_n\tilde{\sigma}_n^*\|}{\|\tilde{\sigma}_n\|\|\tilde{\sigma}_n^*\|} + \frac{\nu}{i\omega} \frac{\|\tilde{\sigma}_n\tilde{\sigma}_n^*/\sigma_n\|}{\|\tilde{\sigma}_n\|\|\tilde{\sigma}_n^*\|}, \tag{A7}$$

where the form of (23) may be recognized. Using (8a), it is easy to verify that

$$\langle \tilde{\mathbf{v}} \cdot \mathbf{e} \rangle = \|\tilde{\sigma}_n\| \tag{A8}$$

and

$$\langle \tilde{\mathbf{v}} \cdot \tilde{\mathbf{v}}^* \rangle = \|\tilde{\sigma}_n\tilde{\sigma}_n^*\|. \tag{A9}$$

Using (9a), we finally verify that

$$-\langle \tilde{\mathbf{v}} \cdot \nabla^2 \tilde{\mathbf{v}}^* \rangle = \|\tilde{\sigma}_n\tilde{\sigma}_n^*/\sigma_n\|. \tag{A10}$$

APPENDIX B: PROOF OF THE IDENTITY (41)

We want to prove the identity

$$\int_{S_p} \mathbf{E} \cdot \nabla \Phi dS = \int_{S_p} \Phi \frac{\partial \mathbf{E}_\beta}{\partial \beta} dS. \tag{B1}$$

It holds that

$$\mathbf{E} \cdot \nabla \Phi = \nabla \cdot (\mathbf{E}\Phi), \tag{B2}$$

because $\nabla \cdot \mathbf{E} = 0$. We may now introduce the Gauss coordinates x_μ on the curved surface S_p , where $\mu = 1, 2, \beta$. Any tensor in the conventional Euclidian coordinates may be expressed in the x_μ system:¹⁹

$$\begin{aligned} \int_{S_p} \nabla \cdot (\mathbf{E}\Phi) dS &= \int_{S_p} [E_\mu \Phi]_{,\mu} dS \\ &= \int_{S_p} [E_i \Phi]_{,i} dS + \int_{S_p} [E_\beta \Phi]_{,\beta} dS, \end{aligned} \tag{B3}$$

where the subscript comma is used for the derivative, and i runs over 1,2 only. Due to the compact character of the field Φ , the third integral in (B3) is zero, so that we find from (B2) and (B3) that

$$\int_{S_p} \mathbf{E} \cdot \nabla \Phi dS = \int_{S_p} E_\beta \frac{\partial \Phi}{\partial \beta} dS + \int_{S_p} \Phi \frac{\partial E_\beta}{\partial \beta} dS. \tag{B4}$$

Because $E_\beta = 0$ on S_p , we obtain the desired result.

¹D. Lafarge, P. Lemarinier, and J. F. Allard, "Dynamic compressibility of air in porous structures at audible frequencies," *J. Acoust. Soc. Am.* **102**, 1995 (1997).
²C. J. Wisse, D. M. J. Smeulders, M. E. H. Van Dongen, and G. E. Chao, "Guided wave modes in porous cylinders: Experimental results," *J. Acoust. Soc. Am.* **112**, 890 (2002).
³D. M. J. Smeulders, R. L. G. M. Eggels, and M. E. H. Van Dongen, "Dynamic permeability: reformulation of theory and new experimental data," *J. Fluid Mech.* **245**, 211 (1992).
⁴D. L. Johnson, J. Koplik, and R. Dashen, "Theory of dynamic permeability and tortuosity in fluid-saturated porous media," *J. Fluid Mech.* **176**, 379 (1987).
⁵P. Sheng and M. Zhou, "Dynamic permeability in porous media," *Phys. Rev. Lett.* **61**, 1591 (1988).
⁶M. Zhou and P. Sheng, "First-principles calculations of dynamic permeability in porous media," *Phys. Rev. B* **39**, 12 027 (1989).
⁷J.-L. Auriault, L. Borne, and R. Chambon, "Dynamics of porous saturated media, checking of the generalized law of Darcy," *J. Acoust. Soc. Am.* **77**, 1641 (1985).
⁸E. Charlaix, A. P. Kushnick, and J. P. Stokes, "Experimental study of dynamic permeability in porous media," *Phys. Rev. Lett.* **61**, 1595 (1988).
⁹S. Kostek, L. M. Schwartz, and D. L. Johnson, "Fluid permeability in porous media: Comparison of electrical estimates with hydrodynamical calculations," *Phys. Rev. B* **45**, 186 (1992).
¹⁰D. M. J. Smeulders, R. R. Van Hassel, M. E. H. Van Dongen, and J. K. M. Jansen, "Similarity of sharp-edged porous media," *Int. J. Eng. Sci.* **32**, 979 (1994).
¹¹M. Firdaouss, J.-L. Guermond, and D. Lafarge, "Some remarks on the acoustic parameters of sharp-edged porous media," *Int. J. Eng. Sci.* **36**, 1035 (1998).
¹²A. Cortis and D. M. J. Smeulders, "On the viscous length scale of wedge-shaped porous media," *Int. J. Eng. Sci.* **39**, 951 (2001).
¹³Y. Achdou and M. Avellaneda, "Influence of pore roughness and pore-size dispersion in estimating the permeability of a porous medium from electrical measurements," *Phys. Fluids A* **4**, 2651 (1992).
¹⁴M. Avellaneda and S. Torquato, "Rigorous links between fluid permeability, electrical conductivity, and relaxation times for transport in porous media," *Phys. Fluids A* **3**, 2529 (1991).
¹⁵L. D. Landau and E. M. Lifschitz, *Fluid Mechanics* (Pergamon, New York, 1959).
¹⁶S. Pride, "Governing equations for the coupled electromagnetics and acoustics of porous media," *Phys. Rev. B* **50**, 15 678 (1994).
¹⁷M. A. Biot, "Theory of propagation of elastic waves in a fluid-saturated porous solid. II. Higher-frequency range," *J. Acoust. Soc. Am.* **28**, 179 (1956).
¹⁸C. Zwikker and C. W. Kosten, *Sound Absorbing Materials* (Elsevier, Amsterdam, 1949).
¹⁹S. Weinberg, *Gravitation and Cosmology: Principles and Applications of the General Theory of Relativity* (Wiley, New York, 1972).
²⁰S. Rebay, "Efficient unstructured mesh generation by means of Delaunay triangulation and Bowyer-Watson algorithm," *J. Comput. Phys.* **106**, 125 (1993).